

# Fabrication and Characterization of Melt-Extracted Co-Based Amorphous Wires

HUAN WANG, DAWEI XING, XIAODONG WANG, and JIANFEI SUN

Amorphous  $\text{Co}_{68.15}\text{Fe}_{4.35}\text{Si}_{12.25}\text{B}_{15.25}$  wires with smooth surface and circular cross section were fabricated by melt extraction technology using a copper wheel with a knife-edge cross section angle of 60 deg. The effect of some process parameters such as wheel circumference velocity, molten alloy feed rate, and temperature on the geometry and weight, *i.e.*, melt extracted layer thickness, of wire was examined carefully. An optimum process parameter to produce high-quality circular wires was presented. A high resolution CCD video camera recorder was used to monitor the changing of the surface shape of molten alloy contacting the wheel tip under different conditions. It was found that the mechanism of the wire formation during the optimum process condition was controlled by the momentum mechanism, while in the low wheel speed region, heat transfer turned out to be a dominant factor. Some characteristics of the circular wires such as amorphous nature and tensile strength were also studied.

DOI: 10.1007/s11661-010-0459-0

© The Minerals, Metals & Materials Society and ASM International 2010

## I. INTRODUCTION

BECAUSE of the excellent giant magnetoimpedance (GMI) effect and great potential application of highly sensitive magnetic sensors, Co-based amorphous wires have been focused on for many years.<sup>[1-3]</sup> To now, Co-based amorphous wires were prepared by several methods such as glass coating, in-water quenching, and melt extraction technology (MET).<sup>[3-5]</sup> Compared with others, the solidification rate of wires prepared by MET is the highest, which leads the wires to express an excellent GMI effect. Thus, MET has been increasingly used to produce Co-based amorphous wires in recent years.

The concept of melt extraction was first introduced by Maringer<sup>[6]</sup> in 1974 to produce metallic fibers. The basic principle is to use a high-speed wheel with a sharp edge to contact the molten alloy surface and then to rapidly extract and cool a molten layer to be wires. Therefore, the solidification rate of metallic wires can reach  $10^5$  to  $10^6$  K/s, and MET has been used to fabricate amorphous wires and a few ceramic fibers, *e.g.*,  $\text{CaO}\cdot\text{Al}_2\text{O}_3$ <sup>[7]</sup> and  $\text{Al}_2\text{O}_3\cdot\text{Y}_2\text{O}_3$ .<sup>[8]</sup> Because it does not require any liquid cooling mediums, MET can also be used to fabricate some high reactivity alloys such as aluminum,<sup>[9]</sup> titanium,<sup>[10]</sup> zirconium,<sup>[11]</sup> and magnesium<sup>[12]</sup> wires.

Surprisingly, contrary to related methods such as melt spinning and planar flow casting, very few reports throw light on the influence of process parameters on the wires' quality, and the formation of wires during melt extraction is far from understood. Inoue<sup>[13]</sup> studied the changes in diameter and roundness for  $\text{Fe}_{75}\text{Si}_{10}\text{B}_{15}$

wires as a function of wheel velocity and molten rising velocity and produced high circular amorphous wires in the high wheel speed region. Lotze<sup>[14]</sup> believed that heat transfer controlled the fiber formation and described a simple solidification model to investigate the fiber formation of eutectic Al-Cu alloy, calculating the heat transfer coefficient and the cooling rates during melt extraction. Anthony<sup>[15]</sup> supposed that the melt-extracted thermal layer must be thicker than the viscous shear layer in the molten and described the vorticity and temperature distribution adjacent to the rotating wheel, which were determined to be unsuitable later by Takeshita.<sup>[16]</sup> Allahverdi *et al.*<sup>[17]</sup> investigated the extraction of ceramics and produced ZAT fibers with diameters ranging from 15 to 30  $\mu\text{m}$  at the low wheel velocity of 1.5 m/s. They believed that the molten layer was extracted by the momentum of the wheel, and the fiber thickness was controlled by the viscosity of molten, *i.e.*, momentum transfer.

Carefully considering the work mentioned previously, it can be seen that detailed extraction experiments are still needed to clarify the role of the process and the formation of wires during melt extraction, so we extracted Co-based amorphous wires under different process parameters and then examined carefully the effect of the processing conditions on the geometry and puddle behavior. The ultimate aim is to determine an optimum process for fabricating fine Co-based amorphous wires with circular cross section and to supply some information to make clear the formation of wires during melt extraction. Some characteristics of the extracted circular wires were also investigated.

## II. EXPERIMENTAL

A quaternary alloy with nominal composition of  $\text{Co}_{68.15}\text{Fe}_{4.35}\text{Si}_{12.25}\text{B}_{15.25}$  alloy was chosen, because it

HUAN WANG and XIAODONG WANG, Doctoral Candidates, DAWEI XING, Associate Professor, and JIANFEI SUN, Professor, are with the School of Materials Science and Engineering, Harbin Institute of Technology, Harbin 150001, People's Republic of China. Contact e-mail: jfsun\_hit@263.net

Manuscript submitted April 5, 2010.

Article published online November 20, 2010

exhibits nearly zero magnetostriction in the amorphous state. The ingot with a diameter of 8 mm was prepared in argon atmosphere by arc melting. The raw materials are pure Co (99.9 pct) and Fe (99.99 pct) metals and pure Si (99.9 pct) and B (99.7 pct) crystals. The Co-based wires were fabricated by melt extraction technology using a copper wheel with diameter of 160 mm and 60 deg knife edge. The linear velocity of the wheel rim ranged from 2 to 40 m/s. The feed rate of the molten changed from 30 to 180  $\mu\text{m/s}$ . The temperature of the molten at various operation conditions was determined by a Raytek integrated ratio infrared thermometer (MR1SB). The slope value of the alloy was selected as 1, based on the suggested data of Co-based alloys at elevated temperature. The contact geometry between the molten and wheel tip under different process parameters was observed using a high resolution CCD video camera recorder (DRS, RDT-16, Peiport Scientific Ltd, Beijing). The amorphous extent of as-cast samples was identified by an X-ray diffractometer (XRD) with Cu  $K_\alpha$  radiation. The geometry of the extracted wires was studied by scanning electron microscopy (SEM). The measurement of mechanical properties was consistent with ASTM standard D3379-75 at a strain rate of  $4.2 \times 10^{-4}$  in air.

### III. RESULTS AND DISCUSSION

#### A. Optimization of Process Parameters

During the optimization of different melt extraction process parameters, wires of three different geometrical morphologies are obtained: one is uniform wire but with concaved track, the second is wire with Rayleigh waves, and the third is fine and uniform wire, as shown in Figures 1(a), (b), and (c), respectively. The diameter of the uniform circular part of wires and the thickness of the nonuniform part of Rayleigh waves are defined as  $d$  and  $h$ , respectively, as shown in Figure 1(b). The dimensions of wires, *i.e.*,  $d$  and  $h$ , are measured for at least 50 wire samples for SEM images to obtain the average for each data point. The weight of the extracted wires, *w*, *i.e.*, extracted layer, was examined for ten samples each with length of 10 cm.

Figure 2 shows the plots of the averaged  $d$ ,  $h$ , and  $w$  vs wheel velocity. The feed rate of the molten fix is 90  $\mu\text{m/s}$  and the initial temperature is 1300 K, about 50 K higher than the melt temperature. The variation of wire diameters vs wheel velocity passes through a maximum and then decreases with the increase of wheel velocity. For the weight of the extracted wires, the minimum of  $w$  occurs at a wheel velocity of 10 m/s, where the gap between  $d$  and  $h$  reaches maximum. These two plots can be divided into three regions according to the wheel speed: (a) low-speed region (2 to 5 m/s), (b) intermediate speed region (5 to 30 m/s), and (c) high-speed region (30 to 40 m/s). At low- and high-speed regions, wires exhibit a uniform diameter, while in the medium region, Rayleigh waves are found and  $h$  decreases with an increase of the wheel velocity. Obviously, there are some fluctuations of  $d$ ,  $h$ , and  $w$  in the medium region. With

an increase in wheel velocity, Rayleigh waves form and become larger; *i.e.*, the difference between  $d$  and  $h$  increases and reaches a maximum at a wheel velocity of 10 m/s, where a larger number of particles formed. The formation of particles, which is not concluded in the weighing procedure, is the main reason for the minimum wire weight.

The effect of wheel circumference velocity was found to be critically important to obtain fine and uniform wires. It was thought previously that the diameter of the wires or the thickness of the ribbon decreases with the increase of the wheel velocity, but in our test, the result is abnormal at low speeds. This phenomenon was also found in the melt extraction of ceramic material by Allahverdi<sup>[7]</sup> and Taha<sup>[17]</sup> in the melt spinning process of Al-Cu alloy. The abnormal behavior at low velocity may be caused by the increasing wheel vibration when the wheel velocity increases within the low-speed range. The deeper the wheel penetrates into the molten, the larger the diameters will be. On the other hand, as the wheel velocity increases (less than 10 m/s), the concave tracks on the extracted wire become wider. Therefore, the increasing of the vibration is the most likely reason for this abnormal behavior. With further increases in velocity ( $V_s > 10$  m/s), the Rayleigh waves become smaller and the thickness of the wires decreases. The formation of the Rayleigh waves can be found elsewhere.<sup>[17]</sup> In the high-speed region ( $V_s > 30$  m/s), fine and uniform wires with a diameter of less than 40  $\mu\text{m}$  are obtained. The production of high-quality wires in the high-speed region has been reported by Inoue<sup>[13]</sup> for the melt extraction of Fe-Si-B and Co-Si-B alloys, but the mechanism of this process needs to be examined more closely. When the molten material contacts the wheel tip, a very thin liquid layer starts to form in the contact area and spreads toward the velocity direction. The entire layer is still liquid in this stage and slips fast on the top of the surface underneath the molten material. Although some heat transferred to the wheel, no massive solidification occurred because of its high speed.

Figure 3 gives the dimension and weight of the wires vs feed rate, while other process parameters remain constant. The diameters of the wires remain constant before 90  $\mu\text{m/s}$ , because of the discontinuousness of the extraction process, and then increase slightly with increasing feed rate. With further increasing feed rate, some ribbon-shaped wires and even particles occurred, which result in the reduction of wire weight. Rayleigh wave and concave form during high feed rate regions, especially in the range of 150 to 180  $\mu\text{m/s}$ . The formation of these two kinds of defects is the result of the contest between the cooling effect of the cooper wheel and the surface tension on the free surface of the wire.

Since temperature alters the molten properties such as surface tension and viscosity, it is reasonable to expect that the thickness of the wire also varies with temperature. Figure 4 shows the effect of temperature on the wire diameter. Although the reported temperatures are not the absolute values because of the unavailable slope, some process rule can also be drawn. The dimensions as well as weight of the wires also pass through a maximum and decrease with the increase of temperature, which is a

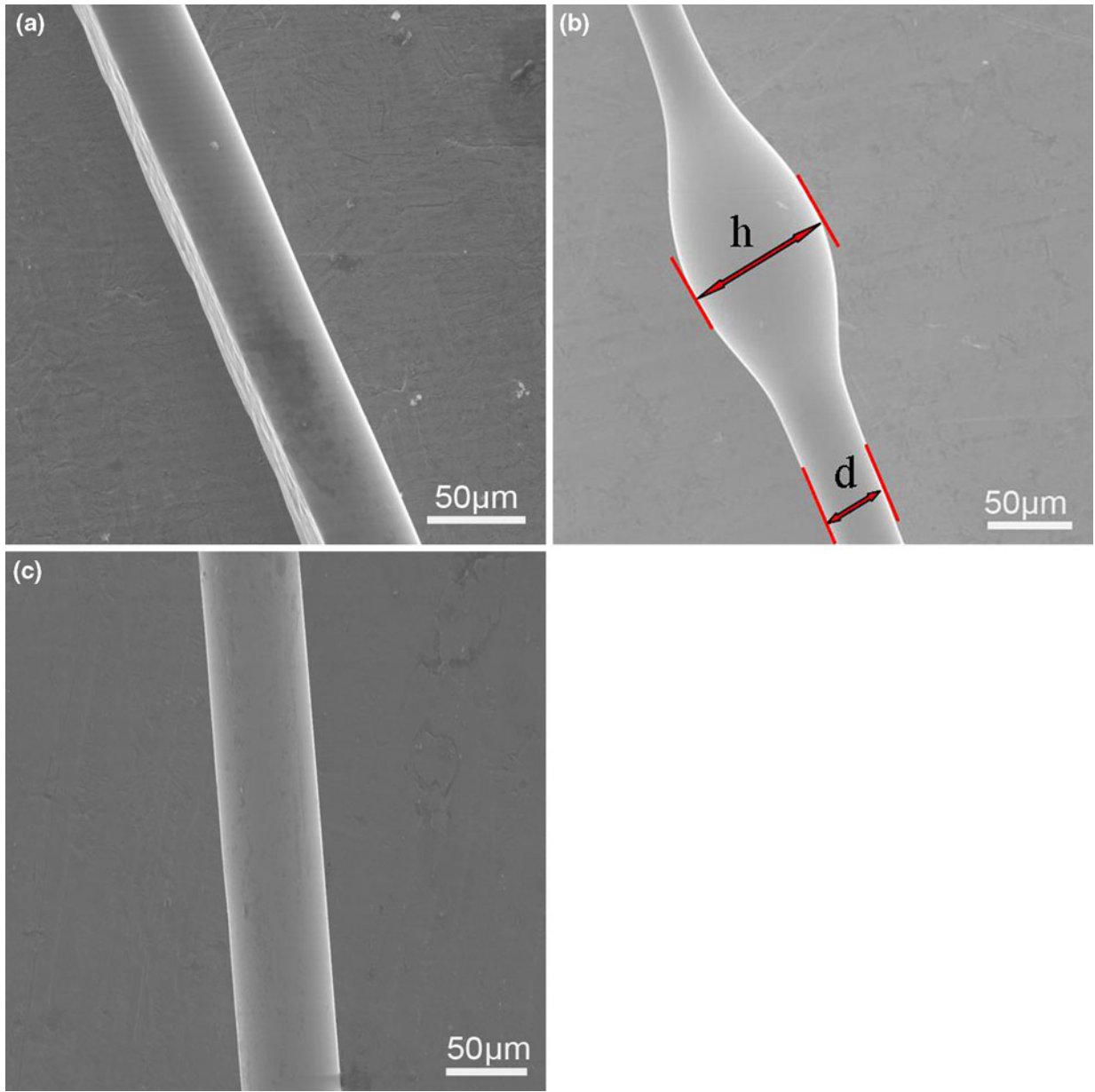


Fig. 1—SEM micrographs of wires at various wheel velocities: (a) 4 m/s, (b) 10 m/s, and (c) 30 m/s.

result of the changes in the liquid properties and dynamic wettability between the wheel and the molten.

The molten feed rate together with the wheel velocity affects the roundness of the wire and the formation of Rayleigh waves obviously. The faster the molten feeds, the thicker it immerses into the copper wheel, which promoted heat transformed into it. When it happened, the molten supercooled below the melt point, and solidification occurred adjacent to the wheel tip, leading to the formation of the concave; meanwhile, on the free surface of the extracted layer, heat transferred to the supercooled region and surface tension acted as a dominant factor, tending to minimize the surface of the liquid layer, and some Rayleigh waves may have occurred when it experienced some unproper cooling rate. So the coexistence of concave and Rayleigh waves

makes the operating window of MET very narrow and limits its application.

#### B. Contact Geometry of the Molten with the Wheel Tip

The contact geometry between the tip of the rotary wheel and molten provides us with some insight into the formation mechanism of melt-extraction metallic wires. Figures 5(a) and (b) show the contact geometry at wheel velocities of 2 and 30 m/s, where uniform wires were fabricated.

From Figure 5(a), due to the surface tension of the molten materials and the decrease in temperature, the dragged molten tends to shrink with lower energy and a gap is seen in the front of the contact area. As the speed increased, as shown in Figure 5(b), the shear force

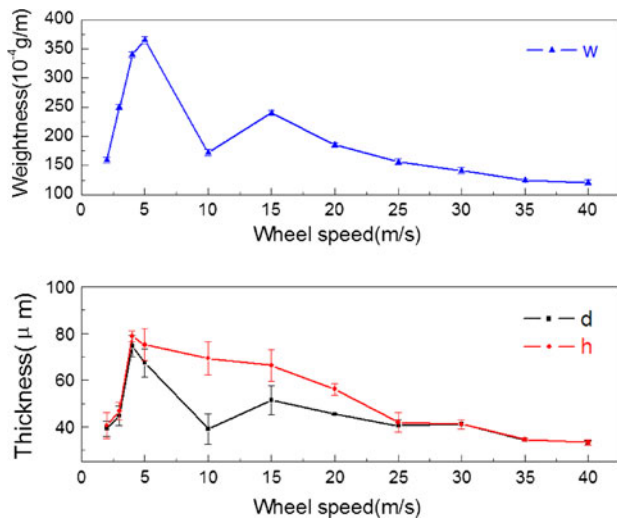


Fig. 2—Variation of  $d$  and  $h$  vs wheel velocity.

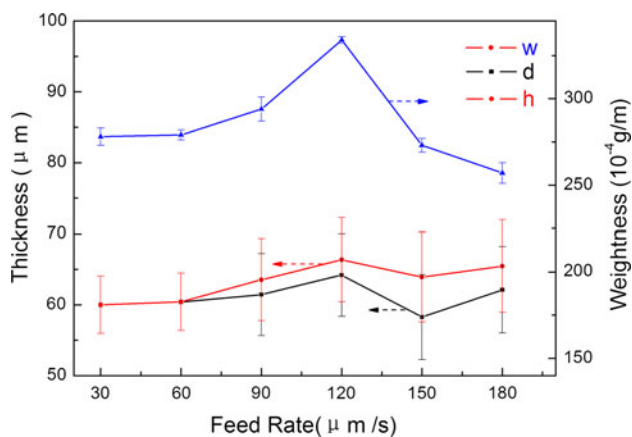


Fig. 3—Changes in diameter and weight as a function of molten alloy feed rate.

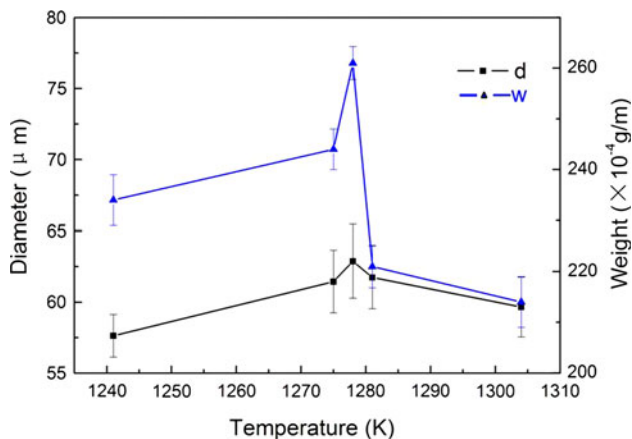


Fig. 4—Variation of  $d$  and  $w$  vs the molten temperature.

between the wheel and the molten became greater; a sharp frontier was seen in front of the contact area, which played an important role in the formation of amorphous wires.

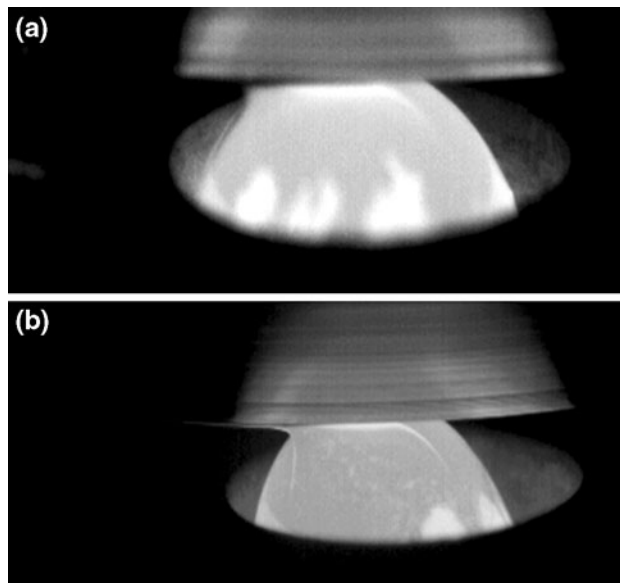


Fig. 5—Contact geometries between molten drop and rotating wheel: (a) 2 m/s and (b) 30 m/s.

In fact, wetting of the copper by molten alloy plays a key role in producing amorphous wires. In an isothermal static wetting, the wettability can be expressed by Young's equation as follows:

$$\cos \theta = (\gamma_{sv} - \gamma_{sl}) / \gamma_{lv}$$

where  $\gamma$  is the surface energy or surface tension; and the subscripts  $s$ ,  $l$ , and  $v$  indicate the solid, liquid, and vapor, respectively. Once the contact interface begins to move, the conditions are generally complicated. This is because the dynamic forces generated by motion change the surface tension, altering the balance in the Young's equation. In the optimization of process parameters, the surface tension of molten  $\gamma_{lv}$  acts as a resistance to limit the fluid of molten and tends to increase as the temperature decreases. In the low velocity region, part of the solidification occurs on the wheel tip and decreases the temperature of the molten. In this region, surface tension changing with temperature acts as a dominant force to produce metallic wires. The mechanism of wire formation may be influenced by the heat transfer from the molten to the wheel tip; in the high-speed region, wettability of this process is promoted by dynamic shear force and overcomes the surface tension obstacle. The contact time  $\Delta t \approx 46$  ms at a wheel velocity of 35 m/s revealed in the high-speed video recorder that no solidification occurred in such a short period of time. In this region, fine and uniform wires with circular cross section were fabricated, which indicates that the wires were in liquid state when they left the molten and the solidification completely took place after they were extracted and flew in the argon atmosphere. This is different from the previous result that solidification is almost completed when the dragout leaves the wheel during the melt spinning of amorphous ribbons. The accelerated layer is almost liquid, which promoted the momentum penetration into the layer. Therefore, it can be concluded that the mechanism of melt



extraction at high-speed regions is controlled by momentum transfer. Supercooled liquid flies in the atmosphere without contacting with any substrate, leading to the suppression of heterogeneous nucleation; at the same time, surface tension acts as a dominant force, which tends to minimize the surface of liquid stream leading to the formation of highly circular cross-sectional amorphous wires.

So the optimum process parameters to fabricate fine and uniform circular wire in our test are as follows: wheel circumference velocity of 30 to 35 m/s, molten alloy feed rate fixed at  $90 \mu\text{m/s}$ , and temperature of the alloy about 50 K higher than the melt temperature. Under the preceding conditions, high-quality wires with

uniform and circular cross section were fabricated, as shown in Figure 6.

### C. Characteristic of the Extracted Wires

The X-ray diffraction patterns taken from the wires with  $d \approx 40$  and  $60 \mu\text{m}$  are shown in Figure 7. It can be seen that both of these two patterns consist only of broad peaks, and no crystalline peaks are found, indicating their amorphous nature. That is, melt extraction technology can be used to fabricate rapidly solidified Co-based amorphous wires.

Since material geometry directly influences its properties, the existence of Rayleigh waves can dramatically degrade the mechanical property of the extracted wire. In our test, uniform wires without Rayleigh wave can be fabricated under two conditions: one is low wheel velocity of less than 10 m/s and diameter of wire about 60 to  $80 \mu\text{m}$ ; and the other is a high-speed region (30 to 40 m/s) with diameter of about 30 to  $40 \mu\text{m}$ . Figures 8(a) through (c) show the tensile strength-strain curve and fracture morphology of these wires with diameters of about 60 and  $40 \mu\text{m}$ , respectively. The tensile strength of the thin uniform circular wire is approximately 3700 MPa, a little higher than the previous results,<sup>[18]</sup> processed by glass-covered amorphous wires, while for the wire with diameter of  $60 \mu\text{m}$ , its tensile property is much lower than the previous one, about 2850 MPa. The higher tensile strength can be explained by the low stress concentration, perfect geometry, and high amorphous nature. From Figures 8(b) and (c), it can be seen that both the fracture figures are composed of two regions: a relatively featureless zone produced by shear slip and a vein pattern produced by the rupture of the cross section remaining after the initial shear displacement. However, the former wire of  $40 \mu\text{m}$  fractures along the maximum shear plain, which is declined by about 45 deg to the tensile direction, and some molten droplets form at the initial part of the vein pattern; for  $60\text{-}\mu\text{m}$  wires, tensile fracture occurs on a shear plane at 90 deg to the

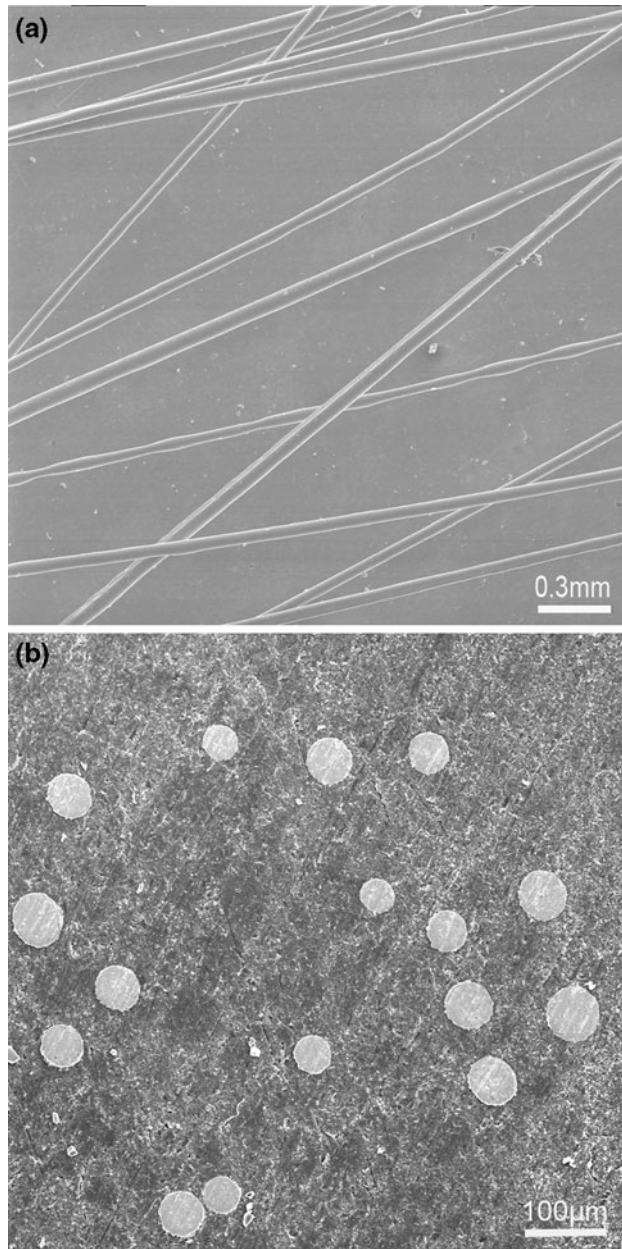


Fig. 6—SEM images of extracted wires at 35 m/s of wheel velocity,  $90 \mu\text{m/s}$  of feeding rate using a copper wheel.

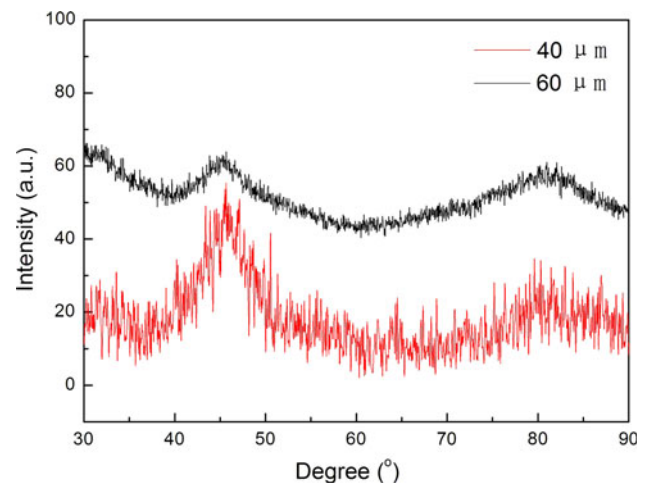


Fig. 7—X-ray diffraction patterns of  $\text{Co}_{68.15}\text{Fe}_{4.35}\text{S}_{112.25}\text{B}_{15.25}$  with diameters of 40 and  $60 \mu\text{m}$ .

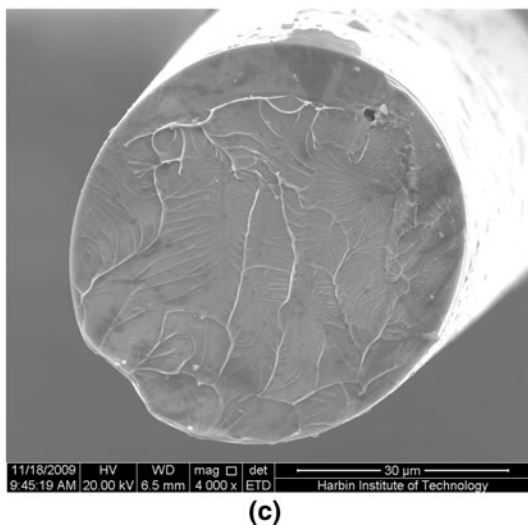
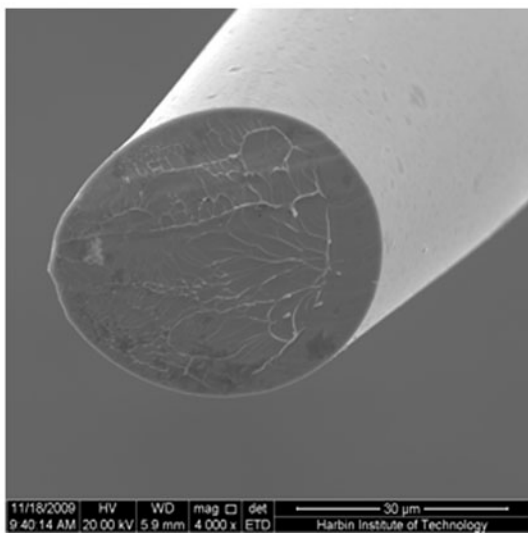
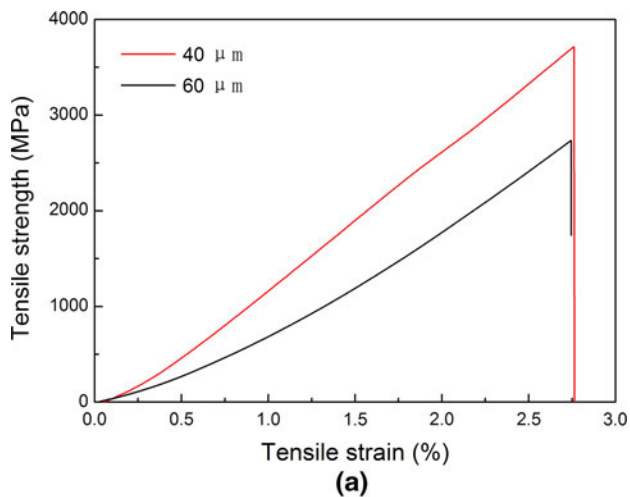


Fig. 8—Tensile strength-strain curve and fracture morphology of the wires with diameters of about 40 and 60  $\mu\text{m}$ .

transverse section. The former wire has a cross-sectional area a little smaller than that of the remaining wires, indicating that some local necking occurred before fracture.

#### IV. CONCLUSIONS

We demonstrate a successful fabrication of Co-based amorphous wires with high geometrical quality directly from molten alloy, using a melt extraction technology with a copper wheel. The effect of process parameters on the geometry of extracted wires was considered. An optimum process parameter to produce high-quality circular wires was presented. Amorphousness and mechanical property of about 40 and 60  $\mu\text{m}$  were identified. A sharp frontier was seen in front of the contact area during optimum process condition, which played an important role in the formation of amorphous wires. It seems both thermal and viscous, *i.e.*, momentum transport mechanism, are involved in the different process conditions. The controlled mechanism in the optimum process region is momentum transport.

#### REFERENCES

1. M. Vazquez and A. Hernando: *J. Phys. D: Appl. Phys.*, 1996, vol. 29 (4), pp. 939–49.
2. L.V. Panina, K. Mohri, T. Uchiyama, M. Noda, and K. Bushida: *IEEE Trans. Magn.*, 1995, vol. 31 (2), pp. 1249–60.
3. H. Chiriac and T.A. Ovari: *Prog. Mater. Sci.*, 1996, vol. 40 (5), pp. 333–407.
4. N.M. Albuquerque: *IEEE Trans. Magn.*, 1995, vol. 31 (2), pp. 1219–23.
5. J. Strom-Olsen: *Mater. Sci. Eng. A*, 1994, vol. 178, pp. 239–43.
6. R.E. Maringer and C.E. Mobley: *J. Vac. Sci. Technol.*, 1974, vol. 11, pp. 1067–71.
7. M. Allahverdi, R.A.L. Drew, and J.O. Strom-Olsen: *J. Mater. Sci.*, 1996, vol. 31 (4), pp. 1035–42.
8. E.A. Aguilar, R.A.L. Drew, B. Saruhan, C. Milz, and B. Hildmann: *Br. Ceram. Trans.*, 2000, vol. 99 (6), pp. 256–59.
9. N.I. Baik, Y. Choi, and K.Y. Kim: *J. Mater. Process. Technol.*, 2005, vol. 168 (1), pp. 62–67.
10. A.G. Kostromov, V.N. Klimentko, M.M. Serov, N.I. Levitskii, S.V. Prishchepov, and B.V. Borisov: *Powder Metall. Met. Ceram.*, 2008, vol. 47 (7–8), pp. 384–88.
11. T. Nagase, K. Kinoshita, and Y. Umakoshi: *Mater. Trans.*, 2008, vol. 49 (6), pp. 1385–94.
12. B. Zberg, E.R. Arata, P.J. Uggowitzer, and J.F. Lfler: *Acta Mater.*, 2009, vol. 57 (11), pp. 3223–31.
13. A. Inoue, A. Katsuya, K. Amiya, and T. Masumoto: *Mater. Trans.*, 1995, vol. 36 (7), pp. 802–09.
14. G. Lotze, G. Stephani, W. Loeser, and H. Fiedler: *Mater. Sci. Eng. A*, 1991, vol. 133, pp. 680–83.
15. T.R. Anthony and H.E. Cline: *J. Appl. Phys.*, 1979, vol. 50 (1), pp. 239–44.
16. K. Takeshita: *Trans. Jpn. Inst. Met.*, 1983, vol. 24 (7), pp. 529–36.
17. M.A. Taha, N.A. El-Mahallawy, and M.F. Abdel-Gaffar: *Mater. Sci. Eng. A*, 1991, vol. 134, pp. 1162–65.
18. H. Chiriac, N. Lupu, V. Dobrea, and S. Corodeanu: *Status Solidi—A*, 2009, vol. 206 (4), pp. 648–51.